Accelerating and abruptly-autofocusing beam waves in the Fresnel zone of antenna arrays

Ioannis Chremmos and George Fikioris and Nikolaos K. Efremidis

Accelerating and abruptly-autofocusing beam waves in the Fresnel zone of antenna arrays

Ioannis D. Chremmos, George Fikioris, and Nikolaos K. Efremidis

Abstract

We introduce the concept of spatially accelerating (curved) beam waves in the Fresnel region of properly designed antenna arrays. These are transversely localized EM waves that propagate in free space in a diffraction-resisting manner, while at the same time laterally shifting their amplitude pattern along a curved trajectory. The proposed beams are the radiowave analogue of Airy and related accelerating optical waves, which, in contrast to their optical counterparts, are produced by the interference of *discrete* radiating elements rather than by the evolution of a continuous wavefront. Two dyadic array configurations are proposed comprising 2D line antennas: linear phased arrays with a power-law phase variation and curved power-law arrays with in-phase radiating elements. Through analysis and numerical simulations, the formation of broadside accelerating beams with power-law trajectories is studied versus the array parameters. Furthermore, the abrupt autofocusing effect, that occurs when beams of this kind interfere with opposite acceleration, is investigated. The concept and the related antenna setups can be of use in radar and wireless communications applications.

1 Introduction

The concept of accelerating wavepackets emerged in 1979 in the context of quantum mechanics [1]. It was then shown that the time-dependent Schrödinger equation for a one-dimensional (1D) free particle ($i\hbar u_t = -\hbar^2 u_{xx}/2m$, m being the mass) accepts the solution

$$u\left(x,t\right)=Ai\left(\kappa x-\frac{\kappa^{4}\hbar^{2}t^{2}}{4m^{2}}\right)\exp\left(i\frac{\kappa^{3}\hbar tx}{2m}-i\frac{\kappa^{6}\hbar^{3}t^{3}}{12m^{3}}\right) \tag{1}$$

where $u(x,0)=Ai(\kappa x)$, Ai is the Airy function and κ (m^{-1}) is an arbitrary real constant. There are two remarkable properties about the solution (1) which is illustrated in Fig. 1(a). First, the shape of the probability density $|u|^2$ remains constant with time, i.e. it represents a wavepacket that evolves *without dispersing*. In fact, (1) is *the only* dispersion-free solution of Schrödinger equation in 1D free space [2] that is localized in the sense $u\rightarrow 0$ as $x\rightarrow\pm\infty$. Second, this wavepacket moves at a *constant acceleration* as implied by the law $x=\kappa^{3}\hbar^{2}t^{2}/4m^{2}$, which is quite peculiar taking into account the absence of forces acting on the particle. This apparent contradiction to Ehrenfest's theorem [3] (the quantum-mechanical analogue of Newton's law of motion) is resolved if one notes that the Airy wavepacket has infinite energy (L^2-norm), hence its centroid ($\|u\|_2^{-1}\int x|u|^2dx$) cannot be defined.

Despite being physically unrealizable, the self-accelerating Airy wavepacket stimulated the interest of physicists and engineers who embarked on the idea of introducing these waves into the field of electromagnetics. The critical breakthrough was in 2007 when the possibility of diffraction-free *optical* Airy beams was proposed [4], based on the equivalence of Schrödinger equation with Helmholtz equation for paraxial optical beams in free space (e.g. [5]). Indeed, for a y-independent EM wave (termed (1+1)D) that propagates in the z direction and varies along x much slower than the wavelength (λ), the Helmholtz equation for any field component reduces to $u_z=iu_{xx}/(2k)$ ($k=2\pi/\lambda$). The latter is often called the *paraxial wave equation* and is identical to the free-particle Schrödinger equation, if the propagation distance is interpreted as time and after appropriate normalization. Taking a step further, it was also found that exponentially truncated Airy wavefronts of the form $u(x,0)=Ai\left(x\right)\exp\left(ax\right)$ ($a>0$ being a small real parameter) evolve like finite-energy approximations of the ideal Airy solution, maintaining a diffraction-resisting (or quasi-diffraction-free) and accelerating quality over long propagation distances compared to the diffraction (or Rayleigh) length [Fig. 1(b)]. For these finite-energy wavepackets too, the acceleration is perceived as a quadratic lateral shift of their intensity pattern, which is an interference phenomenon and not a violation of Ehrenfest's theorem, as their centroid remains fixed with range [6]. Soon, the new optical beams were produced in the laboratory [7] based on the key remark that the function $Ai\left(x\right)\exp\left(ax\right)$ has a closed-form Fourier transform $U\left(\omega\right)=\exp\left[i(\omega+ia)^{3}/3\right]$. Therefore, it can be easily realized in the Fourier

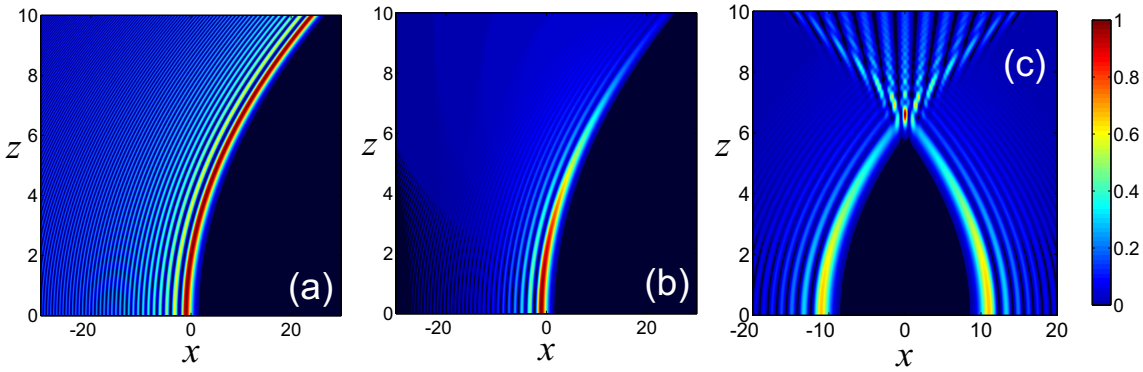

Figure 1: Evolution of (1+1)D Airy waves according to the normalized Schrödinger equation $u_z = iu_{xx}/2$. (a) Ideal Airy wave with $u(x,0) = Ai(x)$. (b) Finite-energy Airy beam with $u(x,0) = Ai(x)\exp(0.05x)$. (c) Two opposite accelerating finite-energy Airy beams with $u(x,0) = Ai(x+10)\exp[0.05(x+10)] + Ai(10-x)\exp[0.05(10-x)]$. The color code represents the normalized intensity $|u|^2$. Variable z represents the propagation distance for paraxial optical beams and time for quantum mechanical wavepackets

space by reflecting the Gaussian beam $\exp(-a\omega^2)$ on a spatial light modulator (SLM) programmed with the cubic phase $\omega^3/3$ and by inverse-Fourier transforming back to the real space by simple means of a lens. (2+1)D Airy optical beams with input wavefronts of the form $Ai(x)Ai(y)$ were also produced by taking advantage of the separability of the wave equation. A thorough operator analysis of the paraxial wave equation also revealed that Airy beams are members of a broader class of accelerating and diffraction-free waves [8]. Interestingly, the trajectory of any wave with these two properties can only be a parabola.

Soon after their inception, accelerating beams (mainly of the Airy type) captured the attention of the optics community by enabling a broad range of applications, such as light trajectory control, wavefront self-healing, optical micromanipulation, diffraction-free plasmon-polaritons, and curved plasma filaments, to name a few. For a self-contained presentation of these applications, the reader is referred to the recent review [9].

One of the impressive possibilities empowered by accelerating waves (and of interest to this paper) is that of producing abruptly autofocusing (AAF) beams [10], namely beams capable of focusing their power right before a target while maintaining a constant and low maximum intensity along the entire path propagated from the source. The associated field structure is based on a circularly symmetric wavefront with Airy radial dependence $Ai(r_0 - r)$. As the radial Airy wavepacket accelerates inward without diffracting, its

intensity remains constant and, just before the point of collapse, the power focuses by orders of magnitude. Experimental tests showed that these beams can outperform standard Gaussians of comparable initial width in scenarios where the laser power has to be tightly focused at long distances [11]. AAF beams have thus far been used for the generation of ablation spots in transparent media [11] and for particle manipulation [12]. An AAF effect with two interfering (1+1)D Airy beams is depicted in Fig. 1(c).

A ray-optics analysis of Airy beams [13] reveals that their spatial acceleration results from the curved caustic that envelopes the rays emitted from the input aperture (Fig. 2). Such a caustic is termed the *fold* in the framework of catastrophe theory [14]. The phase of the Airy wavefront varies as $(-x)^{3/2}$, which makes the rays' slope vary as $(-x)^{1/2}$, which is exactly the law required for a parabolic caustic $x \propto z^2$. This principle can be generalized to produce waves with general power-law trajectories. As shown in [15], a $x \propto z^{\nu}$ caustic is produced by an input wavefront with phase $(-x)^{\beta}$ with the powers connected as $\beta = 2 - \frac{1}{\nu}$. Further extension to arbitrary trajectories, such as exponential and polynomial, was experimentally demonstrated in [16]. Such waves have also been used to define AAF and *autodefocusing* circular beams with arbitrary caustic surfaces of revolution [15, 17]. It should be remembered though that truly diffractionless propagation can only occur along straight or parabolic trajectories, hence waves accelerating along arbitrary trajectories are by definition not diffraction-free.

To date, the concept of accelerating EM waves has remained within the confines of optics and it is for that reason unfamiliar to the vast majority of the radiowaves community. It is of course true that the interest focuses mainly on the far field of antenna systems for wireless communication purposes and less often on phenomena occurring in the near field and, in particular, in the Fresnel zone, as is the case of accelerating beams. Nevertheless, the Fresnel regime is of importance in many radiowave scenarios, as for example in the Fresnel zone clearance of wireless links or in the design of Fresnel zone plate antennas [18]. And undoubtedly, near EM fields are always of interest either for assessing the safety of radiating systems or for manipulating the interference and coupling of wireless devices [19, 20]. Therefore near field phenomena can be of importance in radio engineering too.

The aim of this work is to introduce accelerating EM waves to the radiowaves regime. In principle, this is possible owing to the scaling properties of Maxwell equations. However, in order that the new waves can actually be used in wireless applications, the concept should be adapted to the corresponding disciplines which involve the transmission and reception of EM waves through antenna systems. To this end, we focus on the generation of accelerating EM beams in the Fresnel zone of properly designed antenna

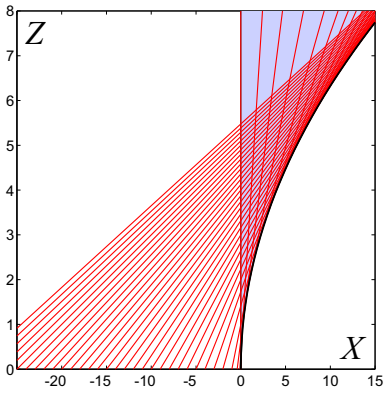

Figure 2: Ray-optics interpretation of an accelerating beam. The input wavefront is confined in the negative x axis and is modulated by the phase $q(x) = -\frac{2}{3}(-\kappa x)^{3/2}$. In normalized coordinates $X = \kappa x$, $Z = \kappa^2 z/k$, the ray starting from $(X, 0)$ has a slope $X^{1/2}$ with respect to the vertical. The rays' envelope rays is the parabolic caustic $X = Z^2/4$, or equivalently $x_c = \kappa^3 z_c^2/4k^2$. The ray equation (3) has two solutions in the shaded area, one in $X < 0$ and zero below the caustic.

arrays. Being essentially a group of independently controllable radiators, an antenna array offers the possibility to produce a *discretized approximation* of the input wavefront associated with Airy and other types of accelerating waves. As will be shown, there are at least two ways for doing so, using either linear phased arrays with an appropriate phase law, or accordingly curved arrays with in-phase elements. For the sake of simplicity, our attention will be mainly on monochromatic transverse-magnetic (TM) waves evolving in 2D and produced by infinitely long and infinitely thin line antennas, leaving some more realistic simulations for the end.

2 Theory

2.1 Accelerating Beam Dynamics

Before addressing antenna arrays, we here go over some basic theory underlying accelerating beams. As mentioned in the introduction, the propagation of (1+1)D paraxial beams is governed by the Schrödinger equation $u_z = iu_{xx}/2k$. In deriving this from Maxwell's equations, it is assumed that the amplitude of any field component, e.g. the electric, can be expressed as $E_y(x, z) = u(x, z)\exp[ik(z - ct)]$ (c being the speed of light) where the envelope varies so slowly that $|u_{zz}| \ll k|u_z|$. Given the boundary condition

on $z = 0$, the solution is obtained in terms of the Fresnel convolution integral [21]

$$u\left(x,z\right) = \frac{1}{\left(i\lambda z\right)^{1/2}} \int_{-\infty}^{+\infty} u\left(\xi,0\right) \exp\left[\frac{ik(x-\xi)^2}{2z}\right] d\xi \tag{2}$$

An accelerating beam results from the formation of a curved caustic which in turn follows from a chirped-phase modulation of the input condition $u(x,0)$ [13]. To see this, assume that the latter can be described by a slowly-varying envelope $A(x)$ modulated by the phase $q(x)$, i.e. $u(x,0) = A(x)\exp(iq(x))$, and substitute into (2), to obtain an integrand of the form $A(\xi)\exp(iQ(\xi))$, where Q is the total phase $Q\left(\xi\right) = q\left(\xi\right) + k(x-\xi)^2/2z$. This form is useful because it lends itself to a stationary-phase approximation of the Fresnel integral, from which the ray-optics interpretation of the propagation phenomenon derives. Explicitly, the condition of phase stationarity ($Q_\xi = 0$) yields

$$x = \xi + z\frac{q'\left(\xi\right)}{k} \tag{3}$$

(the prime denotes a derivative), that is, the ray emitted from point ξ on the input aperture travels at a slope $dx/dz = q'(\xi)/k$ to contribute the main portion of the field observed at (x,z). Inversely, for a given point (x,z), the ray equation (3) must be solved for ξ to determine the contributing ray(s). Without loss of generality, we assume that the input condition is mainly confined in the negative x axis as happens with the Airy function. In addition, we assume that $q'(\xi) > 0$ and $q''(\xi) < 0$ so that the rays are directed toward positive x values and with increasing slope for increasing negative ξ. Then it is easy to see from a graphical presentation that (3) can have zero, one or two roots depending on (x,z) (Fig. 2). The separatrix between the regions with zero and two solutions is a caustic of the fold type, along which a single ξ solution exists and the total phase Q is second-order stationary ($Q_{\xi\xi} = 0$), due to the collapse of two first-order stationary points (see also [22]). From the latter condition and (3), the caustic is parametrically expressed as

$$\left(x_c, z_c\right) = \left(\xi - \frac{q'\left(\xi\right)}{q''\left(\xi\right)}, -\frac{k}{q''\left(\xi\right)}\right) \tag{4}$$

where $\xi < 0$ works here as a parameter. The above formula can be used to design beams with arbitrary caustic trajectories. An interesting case is that of power laws where the phase is of the form $q\left(x\right) = -\gamma(-x)^\beta$ with $\gamma > 0$ and $1 < \beta < 2$. Substituting into (4) and eliminating ξ, the equation

of the caustic is found to be $x_c = \delta z_c^{\nu}$ where $\nu = (2-\beta)^{-1} > 1$ and $\delta = (\nu-1)^{-1}[\gamma\beta\,(\beta-1)\,/k]^{\nu}$. Therefore, a power-law phase results in a power-law caustic. Note also that, since $\beta < 2$, the input wavefront is *sublinearly chirped* and that the closer β gets to 2 (the linear chirp) the higher is the order ν of the caustic.

In the case of an Airy beam (ideal or finite-energy), $u(x,0) \propto Ai(\kappa x)$ (κ controls the transverse beam width) and the Airy function is replaced by its well-known asymptotic expression for large negative arguments $Ai(\kappa x) \sim (-\pi^2\kappa x)^{-1/4}\sin\left[(2/3)(-\kappa x)^{3/2} + \pi/4\right]$. Surprisingly, the latter provides an excellent approximation of the function for $\kappa x < -2$. Breaking the sine function into two complex conjugate exponentials and after the previous discussion, it is easy to see that the term $\propto \exp\left[-i(2/3)(-\kappa x)^{3/2}\right]$ is responsible for the formation of the parabolic caustic $x_c = \kappa^3 z_c^2/4k^2$ (Fig. 2). The complex conjugate term gives rise to symmetric rays propagating toward negative x, as follows from (3) if q is replaced by $-q$. These rays contribute to the total non-diffracting Airy wave in $x < 0$ but not to the formation of its caustic. This is a useful remark because, when working with accelerating beams in practice, one is mainly interested in the field close to the caustic where most of the beam power is confined. For that reason, accelerating *optical* beams are most conveniently produced from chirped traveling-wave input conditions of the form $\propto \exp[iq(x)]$ [16, 17], rather than from chirped standing waves $\propto \sin(q(x))$ which are more difficult to produce experimentally. Interestingly, with antenna arrays, traveling and standing input conditions can be implemented with equal effort, as we will see.

Finally it is interesting to see how the field in the neighborhood of a fold caustic can be determined analytically. To this end, we consider an arbitrary point (x_c, z_c) on the caustic and expand $Q(\xi, x)$ in a Taylor series for small increments $\Delta\xi, \Delta x$ around (ξ_c, x_c), where ξ_c is the corresponding (unique) solution of (3) and $z = z_c$ is fixed. We obtain up to third order

$$\begin{array}{c} Q\left(\xi_c+\Delta\xi, x_c+\Delta x\right) = \left[Q^c + Q_x^c\Delta x + \frac{Q_{xx}^c}{2}(\Delta x)^2\right] \\ +Q_{\xi x}^c\Delta x\Delta\xi + \frac{Q_{\xi\xi\xi}^c}{6}(\Delta\xi)^3 + o\left((\Delta\xi)^3\right) \end{array} \tag{5}$$

where the superscript c means that the function is evaluated at (x_c, z_c) and we have also taken into account that $Q_\xi^c = Q_{\xi\xi}^c = 0$ due to the second-order stationarity of Q at ξ_c. Also, $Q_{\xi\xi x}^c = Q_{\xi xx}^c = Q_{xxx}^c = 0$, $Q_{\xi x}^c = -k/z_c = q''(\xi_c)$ and $Q_{\xi\xi\xi}^c = q'''(\xi_c)$ are obvious from the explicit expression of Q. Substituting (5) into (2) and assuming a slow variation of $A(\xi)$, we obtain after integrating over $\Delta\xi$

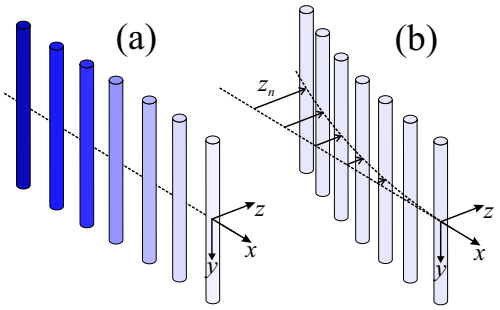

Figure 3: Two antenna array concepts for producing accelerating beams. (a) A linear phased array of equispaced elements with a chirp phase variation indicated by a color gradient. (b) A curved array of in-phase elements. The arrows indicate the z-displacement of the elements.

$$u(x_c + \Delta x, z_c) \approx \frac{2\pi A_c e^{i\theta(\Delta x)}}{(iz_c\lambda)^{1/2}(q_c'''/2)^{1/3}} Ai\left(\frac{q_c'' \Delta x}{(q_c'''/2)^{1/3}}\right) \tag{6}$$

where the subscript c means that the function is evaluated at ξ_c, $\theta(\Delta x)$ is the term in brackets in (5) and we have also used the inverse Fourier transform of the Airy function [23]. Therefore the field near the caustic is distributed like an Airy function irrespective of the caustic's shape. Additionally, (6) shows that the width of this Airy-like beam generally varies with ξ_c, or equivalently with the propagation distance z_c, in agreement with our previous comment that accelerating beams with arbitrary trajectories are generally not diffraction-free. Quasi-diffractionless propagation occurs only when $q_c''/(q_c''')^{1/3}$ is independent of ξ_c, which is easily integrated to yield $q(\xi_c) = -\gamma(-\xi_c)^{3/2} + \mu\xi_c$ with $\gamma > 0$ and μ real. This is exactly the phase modulation of an Airy beam plus a linear phase that simply alters its initial launch angle and is usually used to control the beam trajectory in a ballistic manner [9]). We have thus confirmed in a simple way that diffractionless propagation of paraxial accelerating beams can only occur along parabolic trajectories (refer to [8] for a rigorous proof).

2.2 Antenna arrays

We now proceed to see how accelerated radio beams can be produced by the interference of discrete radiating elements. Consider the setting of Fig. 3(a) or (b), where an array of N parallel ideal line antennas radiate monochromatic TM waves. The electric field observed at any point (x, z) is expressed as

$$E_y(x,z) = \sum_{n=1}^{N} I_n H_0^{(1)}\left(k\left[(x-x_n)^2 + (z-z_n)^2\right]^{1/2}\right) \tag{7}$$

where (x_n, z_n) is the position of the n-th antenna, i_n is the complex amplitude of its electric current (in amperes), and $I_n = -(kZ/4)i_n$, where Z is the wave impedance of free space. Also, $H_0^{(1)}$ is the Hankel function of the first kind in concordance with the time dependence $\exp(-ikct)$. Note that for a linear array $z_n = 0$. To handle (7), we replace the Hankel function by its well-known large-argument formula $H_0^{(1)}(kr) \sim (2/i\pi kr)^{1/2}\exp(ikr)$ [23]. In fact, this expression provides an excellent approximation of $H_0^{(1)}(kr)$ for $kr > 2$ and thus can be used interchangeably for distances $r > \lambda$, which is perfect for all practical calculations.

In order to design accelerating beams, we have to express in a convenient form the field radiated produced in the Fresnel zone of the array. According to the antenna designers' rule of thumb, this zone exceeds up to a distance kD^2/π, which roughly delimits the transition to the Fraunhofer (far-field) region of an antenna with maximum dimension D [24]. For accurate field calculations, the critical point is to treat correctly the phase $k|(x,z)-(x_n,z_n)|$ with which each element contributes to the total field at (x,z). Our focus here is on broadside beams, i.e. emitted perpendicular to the array axis, that propagate in a *paraxial* manner, i.e. with small transverse wavevector components. We find that the most appropriate approach draws from optical Fresnel diffraction [21]. In this context, the phase is approximated as

$$\begin{aligned} k\left[(x-x_n)^2 + (z-z_n)^2\right]^{1/2} \approx \\ k|z| + \frac{k(x-x_n)^2}{2|z|} - \mathrm{sgn}(z)\, kz_n \end{aligned} \tag{8}$$

where propagation toward $z > 0$ or $z < 0$ has been accounted for. Note that the term $kz_n^2/2|z|$ has been ignored, since z_n will be of the order of few λ. In general, the approximation (8) holds under the condition $|z_n| \ll |x - x_n| \ll |z|$, i.e. when the transverse array dimension is much larger than the wavelength which in turn is comparable to the z displacement of the elements (if $z_n \neq 0$). Note also that, since we are interested in broadside beams, z is the large parameter in (8). This is different from the standard antenna engineering approach which involves Taylor-expanding the phase in powers of r_n/r $[r = (x^2+y^2)^{1/2}, r_n = (x_n^2+y_n^2)^{1/2}]$ and is appropriate for monitoring the EM field at increasing distances r all around the antenna. Being an asymptotic approximation for large z, (8) is also increasingly accurate throughout the far-field region and for that reason appropriate for all practical calculations.

In addition to the phase, the amplitudes of the field terms have to be approximated. In Fresnel diffraction, the amplitude is handled similarly to antenna radiation problems, where all distances are set equal to r, which can be here approximated by $|z|$. After the above, (7) yields

$$E_y(x,z) \cong \frac{\pi^{-1}\lambda \mathrm{e}^{ik|z|}}{(i\lambda|z|)^{1/2}} \sum_{n=1}^{N} I_n \mathrm{e}^{-i\mathrm{sgn}(z)kz_n} \mathrm{e}^{\frac{ik(x-x_n)^2}{2|z|}} \tag{9}$$

The result shows that the cylindrical wavefronts emitted by each array element behave in the Fresnel region like exponentials with a quadratic phase, exactly in the same way that a short circular arc can be locally approximated by a parabola. Additionally, if an element is displaced by z_n along the propagation axis, its field contribution is advanced or delayed in time approximately by $|z_n|/c$, as implied by the extra phase $\pm k|z_n|$. Now by comparing (9) and (2), it is apparent that the total array field provides a *discretized* approximation to the evolution of a paraxial beam. The analogy is apparent if the continuous variable ξ is discretized by the element positions x_n and the continuous boundary condition $u(\xi,0)$ by the phase-modulated current amplitudes $I_n \exp(\mp ikz_n)$.

It is now obvious how the array should be designed to produce accelerating beams. A first possibility is to have a linear array with currents that are tuned to discretize the chirped input condition, i.e. $I_n = u(x_n,0)$ (Fig. 2(a)). Individual attenuating and phase-shifting circuits must be attached to each element for this purpose. The input condition can be either standing, e.g. $I_n \propto Ai(\kappa x_n)\exp(\kappa x_n)$, or traveling, e.g. $I_n = A(x_n)\exp(iq(x_n))$. With this configuration, the x axis is a symmetry axis and two mirror-symmetric beams are produced in the $z>0$ and $z<0$ half-spaces.

A second possibility, suggested by (9), is to let the array elements radiate in unison and assign the phase modulation to their z_n displacements, as shown in Fig.3(b). This configuration can only discretize traveling input conditions and produces an asymmetric field distribution. To produce an accelerating beam in the $z>0$ or $z<0$ half-space, the displacements must satisfy $z_n = \mp q(x_n)/k$, respectively. For a caustic like that of Fig. 2 we get $z_n > 0$, i.e. the array bends toward the half-space in which the accelerating beam evolves. Such a design relieves the need for phase-shifting circuits, which is a significant reduction in the complexity of the antenna feed system. Individual attenuators may still be used to modulate the current amplitudes according to $I_n = A(x_n)$, keeping though in mind that this envelope function can be chosen quite freely not affecting the beam's trajectory. Moreover, the curved shape of the array may be advantageous in applications where a *conformal* design is desirable. Additional freedom in shaping the array

exists if one notes that the displacements z_n can also be wrapped *modulo* λ, as the exponents $\exp(\pm ikz_n)$ remain intact. This results in a scattered-like distribution of the elements within a λ-wide strip adjacent to the x axis.

It should be stressed that the above designs are straightforward to implement if the mutual coupling between the array elements is negligible, which is a realistic assumption when the elements are several wavelengths apart. This becomes evident if one realizes that paraxial EM beams vary in the transverse direction on a length scale $\kappa^{-1} \gg \lambda$. For example, the finite-energy Airy wavefront $Ai(\kappa x)\exp(a\kappa x)$ has a Fourier transform $\propto \exp(-a\omega^2/\kappa^2)$, namely a (spatial) bandwidth $B \approx 2\kappa/\sqrt{a}$. Since the array performs a sampling of this wavefront, an upper limit for the inter-element spacing (s) is provided by the Nyquist rate $s < \pi/B = \pi\sqrt{a}/2\kappa$. Now a is typically in the range 0.05-0.2 [4], while $\kappa^{-1} > 10\lambda$, which obviously allows the elements to be few to several wavelengths apart. Under these conditions, each element can be treated as being isolated and its driving voltage should simply be $v_n = i_n Z_{nn}$, where Z_{nn} is its self-impedance. Nevertheless, such a convenience does not come for free. Increasing the inter-element spacing results in the emission of an increasing number of secondary (non-broadside) caustics, at the angles dictated by the diffraction orders of the array as a grating $\sin\theta_m = m\lambda/s$, $m = \pm 1, \pm 2, ...$, where θ is with respect to the z axis [24]. Suppressing all these grating lobes requires that $s < \lambda$, hence a large number of elements is needed to sample a paraxial wavefront. In addition, mutual coupling has to be taken into account and the voltage excitations have to be determined using the complete interaction matrix of the elements mutual impedances Z_{mn}. Finally note that, even in the absence of higher-order diffraction (when $s < \lambda$), there may still be some appreciable power radiated parallel to the array. The field of these *endfire* beams is proportional to $\sum_n I_n \exp(\mp ikx_n)$ for $x \to \pm\infty$, and it can be shown to vanish under the more stringent condition $s < \lambda(1 + B/k)^{-1}$ (proof omitted). The final choice of the spacing is thus left to the designer's trade-off.

2.3 Numerical examples

In this section the proposed idea is demonstrated numerically. The logic underlying the examples is simple. For a given accelerating beam, the array is designed according to the explained analogy between (2) and (9), adopting either the linear or the curved array configuration. For a fair evaluation, the resulting parameters (I_n and x_n) are substituted into the *rigorous* expression (7) and the produced electric field is plotted from the antenna to the Fresnel zone.

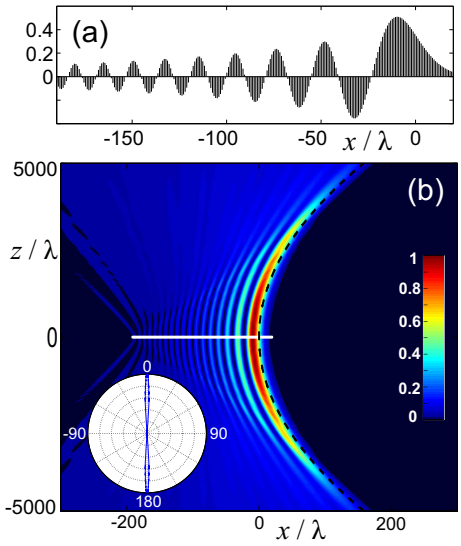

Figure 4: A linear array producing a finite-energy Airy beam. (a) The current amplitudes are $I_n = Ai(0.1\lambda^{-1}x_n)\exp(0.005\lambda^{-1}x_n)$, with the element sites at $x_n = (20 - 0.85n)\lambda$, $n = 0, 1, ..., 249$. (a) Time-averaged electric-field energy density $\epsilon_0|E_y|^2/4$ scaled to its maximum value. The dashed curve is the analytically expected caustic $x = z^2/16000\pi^2$ (x, z in wavelength units). Also indicated with white dots are the radiating elements, appearing like a line segment due to their dense spacing. The inset shows the far-field radiation pattern.

As a first example, consider a linear array that produces a broadside finite-energy Airy beam with $a = 0.05$, $\kappa = (10\lambda)^{-1}$ (bandwidth $B \approx 0.14k$), under the stringent specification of suppressed higher-order and endfire beams. According to the previous discussion, the array spacing is taken $s = 0.85\lambda$. With this sampling rate, a number of $N = 250$ elements has been chosen to allow 18 amplitude extrema of the discretized Airy function. The distribution of current amplitudes across the array is shown in Fig. 4(a), while Fig. 4(b) depicts the result of (7) in terms of the time-averaged electric-field energy density. The radiation pattern is also shown in the inset. The image clearly verifies our expectations for the formation of two mirror-symmetric Airy beams, with respect to the array plane, writing a parabola in space. Note that, due to its paraxial nature, the beam evolves much slower in the z (covering thousands of λ) than in the x direction. Note also the absence of endfire or higher diffraction order radiation, due to the chosen spacing s. It might also be interesting to mention that, for this array with length $D \approx 200\lambda$, the reactive near-field region extends to around $0.62(D^3/\lambda)^{1/2} \approx 1750\lambda$, while

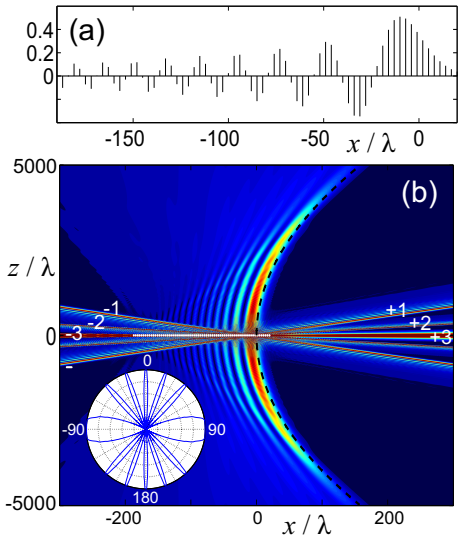

Figure 5: A linear array producing a finite-energy Airy beam. (a) The current amplitudes $I_n = Ai(0.1\lambda^{-1}x_n)\exp(0.005\lambda^{-1}x_n)$, with the element sites at $x_n = (20-3n)\lambda$, $n = 0, 1, ..., 69$. (a) Time-averaged electric-field energy density. The dashed curve is the analytically expected caustic $x = z^2/16000\pi^2$ (x, z in wavelength units). The signed numbers $\pm1, \pm2, \pm3$ indicate the diffraction order of the corresponding beams. The white dots are the array elements. The inset shows the far-field radiation pattern.

the radiating near-field (or Fresnel) region to $2D^2/\lambda = 80000\lambda$ [24]. Hence the formation of the accelerating beam is clearly a near-field phenomenon.

Let us now see the effect of producing the same Airy beam under a less stringent specification for the inter-element spacing. This is the case of Fig. 5 where $s = 3\lambda$, which is around 1.17 times the Nyquist spacing π/B. Fewer elements ($N = 70$) are now required to discretize the same extent of the Airy function. In addition to the desired broadside Airy beam, a number of higher-order grating beams now emerge at angles $19^0, 42^0$ and 90^0 (endfire) with respect to the (positive or negative) z axis (radiation pattern in the inset). A closer look at these beams reveals that they are too accelerating along parabolas. To see this, rotate the frame of coordinates by the corresponding diffraction angle θ_m, whereby the element positions become $(x_n', z_n') = (x_n\cos\theta_m, x_n\sin\theta_m)$. By manipulating the phase in the new frame (x', z') for large z' in a way similar to (8) and noting that $kz_n' = -2mn\pi$ (grating condition), one finds the same equation with the broadside beam ($\theta_0 = 0$) except a factor $(\cos(\theta_m))^{-1}$ that stretches the parabola in the x' direction. A more detailed analysis of these beams is beyond the scope of this introductory paper. What is here to be emphasized is that the spacing (and number

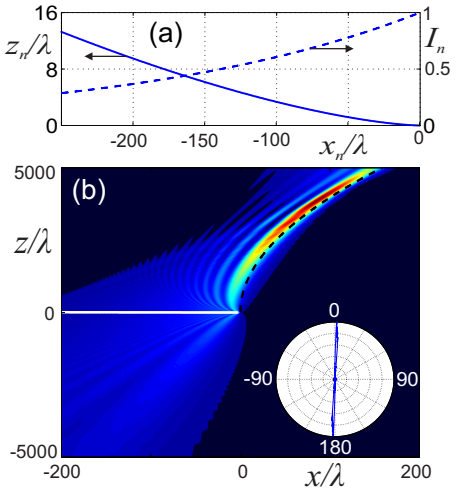

Figure 6: A curved array of in-phase elements producing a parabolic accelerating beam. (a) Solid line (left ordinate): The elements lie on the curve $z_n = (\lambda/3\pi)(-0.1\lambda^{-1}x_n)^{3/2}$, where $x_n = -0.85\lambda n$ and $n = 1, 2, ..., 299$. Dashed line (right ordinate): Exponentially decaying current amplitudes. (b) Electric-field energy density. The dashed line is the parabolic caustic $x = z^2/16000\pi^2$ (x, z in wavelengths). The white dots are the array elements. The inset shows the far-field radiation pattern.

of elements) of the array should be chosen by the designer on the base of a trade-off: larger spacings result in less and weaker-coupled elements but also in radiated power lost in grating lobes.

Next we examine the formation of a beam with the same parabolic trajectory using a curved array of in-phase elements, i.e. $I_n = A_n$, A_n being real and exponentially decaying. According to Section 2, the displacements z_n should obey $z_n = -q(x_n)/k$ where the phase follows the 3/2-chirp of the Airy function, i.e. $q(x_n) = -(2/3)(-\kappa x_n)^{3/2}$. The result is shown in Fig. 6 for $\kappa = (10\lambda)^{-1}$, $x_n = -0.85n\lambda$ and $N = 300$ elements. Note that, due to the break of symmetry with respect to the $z = 0$ plane, the beam forms only in $z > 0$. Indeed, for the waves evolving in $z < 0$, the phase chirp is opposite (due to the sign function in (9)) hence the rays fan out instead of converging to create a caustic. Notable is also the difference between the energy images of Fig. 4(b) and Fig. 6(b). In the former case, the element currents discretize the exact Airy wavefront resulting in an almost perfect approximation of the finite-energy Airy beam. In the latter case, the array reproduces only the rays responsible for the creation of the caustic, hence the beam is Airy-like only close to this curve.

Going beyond parabolic trajectories, Fig. 7 examines the case of a beam

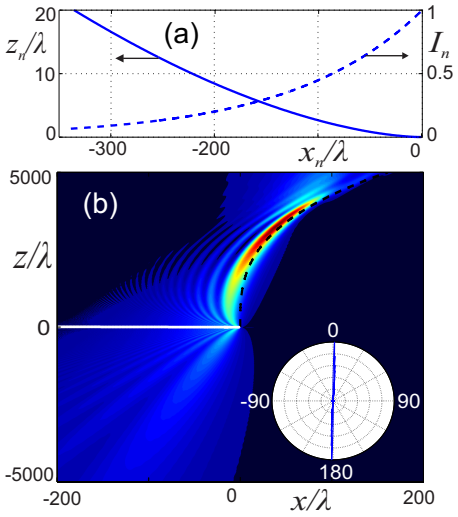

Figure 7: A curved array of in-phase elements producing a cubic accelerating beam. (a) Solid line (left ordinate): The elements lie on the curve $z_n = (9\lambda/50\pi)(-0.1\lambda^{-1}x_n)^{5/3}$, where $x_n = -0.85\lambda n$ and $n = 1, 2, ..., 399$. Dashed line (right ordinate): Exponentially decaying current amplitudes. (b) Electric-field energy density. The dashed line is the cubic caustic $x = z^3/2.5 \times 10^7\pi^3$ (x, z in wavelengths). The white dots are the array elements. The inset shows the far-field radiation pattern.

with a cubic caustic. This is produced by a curved array whose z_n follow a 5/3-power law ($\beta = 2 - 1/3$). Comparing with Fig. 6, one sees that, while the width of the field lobe near the parabolic caustic remains almost constant over several thousands of wavelengths, the lobe near the cubic caustic gets narrower. This agrees with (6) and the discussed diffraction-resisting quality of parabolic caustics.

Regarding the radiation diagrams of the previous arrays, it might be interesting to note that they are quite rippled (as a closer look at the polar plots reveals). It should be stressed that such arrays are designed to produce curved beams in the Fresnel zone, a requirement that is generally incompatible with producing a smooth radiation diagram. Also note that the formation of a curved beam is a rays' interference phenomenon that is not necessarily accompanied with higher directivity of the array toward this direction. Hence Figs. 6 and 7 should not mislead one to assume that most of the power is radiated toward $z > 0$ where the caustic forms, since there is an almost equally strong backward lobe toward $z < 0$, as the radiation diagram shows. Achieving a desired field pattern both in the Fresnel and in the Fraunhofer region is a much more complicated task that certainly merits

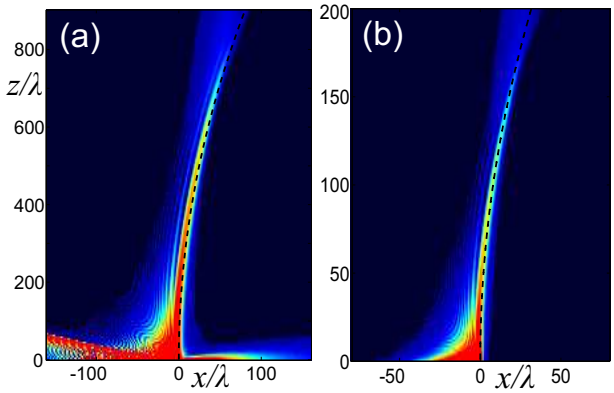

Figure 8: Electric field energy density $|E_y|^2$ on the H-plane of a linear array of 150 half-wave dipoles with (a) λ and (b) $\lambda/2$ spacing. In both cases the dipoles are center driven by voltages $V_n = \exp\left(0.1\kappa x_n + i\frac{2}{3}(-\kappa x_n)^{3/2}\right)$ where $\kappa = 0.25\lambda$ in (a) and 0.5λ in (b). The full EM simulation has been performed in $z \geq \lambda$ to avoid excessively high field values. Some pixelization of the images is evident due to the used 200×200 spatial grid. Superposed with dashed curve are the analytically expected parabolic caustics.

further investigation.

Let us now consider a realistic setting of a linear phased array of half-wave ($\lambda/2$) dipoles. A full EM thin-wire simulation [24] is applied in order to take into account the effects of mutual coupling between the elements. The dipoles are assumed to be center-driven by voltages that obey the 3/2-chirp phase law of Fig. 6, which act as the inputs to our system. Figure 8 depicts the obtained electric-field energy density $|E_y|^2$ on the H-plane $y = 0$ of the array for two different array spacings λ and $\lambda/2$. In both cases the formation of the Airy-like beam is clear. Some distortion is evident particularly in the near field which is due to the fact that, as mutual impedances between elements increase, the currents I_n are no longer proportional to the applied voltages V_n. After experimenting with several settings, we could say as a rule of thumb that fine accelerating beams can be produced by half-wave dipole arrays with spacings as low as $\lambda/2$.

We finally investigate the possibility of AAF beams through the interference of two arrays producing opposite accelerating beams, like that of Fig. 1(c). An example is shown in Fig. 8(a), where two finite-energy Airy beams produced by two identical arrays with the parameters of Fig. 4 collide. What is interesting in such a focusing scenario is to monitor the maximum intensity of the wave in the transverse plane versus the propagation distance, i.e. $I_{max}(z) = \max_x(|E_y(x,z)|^2)$. As shown in Fig. 9(c), I_{max} exhibits a behaviour

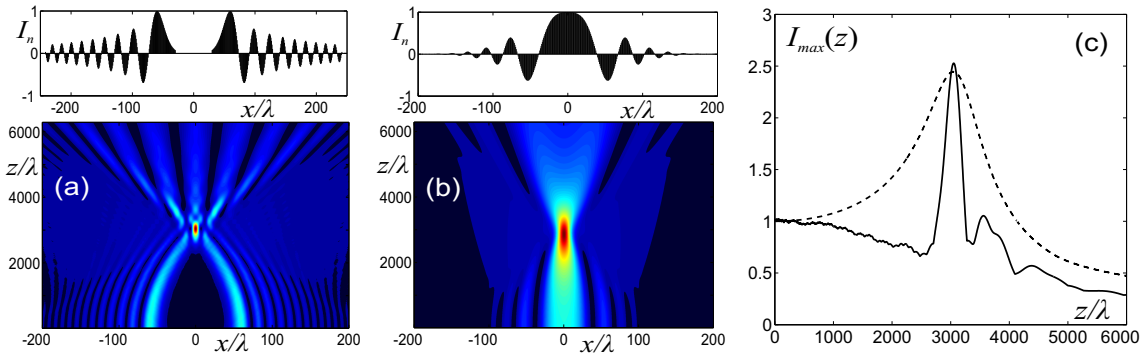

Figure 9: (a) AAF waves from interfering arrays producing opposite accelerating Airy beams. The array parameters are the same with Fig. 4 and their separation is 60 wavelengths. (b) Focusing with an array of 500 elements and currents $I_n = \exp\left(-x_n^2/(80\lambda)^2\right)\cos\left(kx_n^2/6000\lambda\right)$. The top plots show the array currents. (c) Maximum intensity versus propagation distance for the beams of (a) (solid line) and (b) (dashed line).

analogue to AAF optical beams of the circular-Airy kind [10], namely it maintains a fairly constant value and focuses abruptly only right before the target. In optics, the performance of such beams is appreciated by comparing them to standard Gaussian beams which focus due to the quadratic phase modulation obtained after passing through a thin spherical lens. An antenna array counterpart of that case would be an array centered at $x = 0$ with currents of the form $I_n = \exp\left(-x_n^2/w^2\right)\cos\left(kx_n^2/2f\right)$, where f is the intended focal distance. The result is shown in Fig. 9(b) and the corresponding I_{max} is superposed in Fig. 9(c). For a fair comparison, the e^{-1} width w was chosen so that the L^2-norm of the currents $(\sum_n |I_n|^2)$ is the same for the two arrays, assuming the same number of elements (and spacing) and that both current sets are scaled so that $\max(|I_n|) = 1$. This is analogous to two optical beams with equal power. Furthermore notice that the quadratic phase was imposed on the currents through a "standing" cosine factor instead of a "traveling" exponential factor, so that we fairly compare two waves with a "standing" input conditions (recall that half of the rays emanating from a standing input condition fan out without contributing to focusing). The comparison clearly illustrates the difference between AAF from interfering ray caustics and the (classic) smooth Lorentzian focusing from a converging Gaussian pencil of rays.

3 Conclusion

Accelerating EM beams have been introduced into the radiowaves realm. After making a review of accelerating waves in the optics domain, we have gone through the basic theory underlying the evolution of these waves in the Fresnel regime of diffraction. By applying the same reasoning to the 2D field radiated in the Fresnel zone of line antenna arrays, we have physically been led to a simple method to generate accelerating radio beams with pre-specified caustic trajectories. The array should be designed so that the element currents perform a discretization (or sampling) of the continuous wavefront that is associated with an accelerating beam through the Fresnel convolution integral. Linear and curved array configurations have been proposed. In the second type, the elements radiate in phase, while the chirped phase variation is assigned to their arrangement along a power-law curve in space. Proof-of-concept numerical examples have provided positive evidence for the feasibility of these designs. Design issues related to the sampling rate and the suppression of endfire and grating lobes have also been addressed. We have finally showed that when such beams interfere at opposite accelerations, an effect is obtained similar to the recently introduced AAF optical beams. Several issues are still to be addressed in future works, such as the (non-trivial) extention to 3D radiation from dipole arrays, the efficient design under mutual inter-element coupling, the simultaneous optimization of the far-field pattern and the extreme beam bending at non-paraxial angles, which is already attracting attention in the optics field [25, 26, 27]. Emerging ideas for accelerating optical beams with symmetric Bessel-like profiles [28, 29] can also be explored in the RF domain.

Accelerating beams have so far been studied only within the domain of optics. The present work aims to draw the attention of the radio-engineering community to this intriguing class of EM waves by investigating simple 2D antenna configurations capable of producing them. By virtue of their diffraction-resisting quality, such waves (and mainly of the Airy type) can be useful in wireless communications or remote sensing applications for delivering power within tightly focused beams at a Fresnel range.

Acknowledgment

I.D.C. was supported by the project "Archimedes Center for Modeling, Analysis and Computation" (ACMAC, FP7-REGPOT-2009-1). N.K.E. was supported by the action "ARISTEIA" in the context of the Operational Programme "Education and Lifelong Learning" that is co-funded by the Euro-

pean Social Fund and National Resources.

References

[1] M. Berry and N. Balazs, "Non-spreading wavepackets," *Am. J. Phys.*, vol. 47, no. 3, pp. 264–267, 1979.

[2] K. Unnikrishnan and A. R. P. Rau, "Uniqueness of the Airy packet in quantum mechanics," *American Journal of Physics*, vol. 64, no. 8, pp. 1034–1035, 1996.

[3] A. Messiah, *Quantum mechanics*. No. τ. 1 in Quantum Mechanics, North-Holland Pub. Co., 1961.

[4] G. A. Siviloglou and D. N. Christodoulides, "Accelerating finite energy airy beams," *Opt. Lett.*, vol. 32, pp. 979–981, Apr 2007.

[5] D. Dragoman and M. Dragoman, *Quantum-Classical Analogies*. The Frontiers Collection, Springer, 2004.

[6] I. M. Besieris and A. M. Shaarawi, "A note on an accelerating finite energy airy beam," *Opt. Lett.*, vol. 32, pp. 2447–2449, Aug 2007.

[7] G. A. Siviloglou, J. Broky, A. Dogariu, and D. N. Christodoulides, "Ballistic dynamics of airy beams," *Opt. Lett.*, vol. 33, pp. 207–209, Feb 2008.

[8] M. A. Bandres, "Accelerating beams," *Opt. Lett.*, vol. 34, pp. 3791–3793, Dec 2009.

[9] Y. Hu, G. Siviloglou, P. Zhang, N. Efremidis, D. Christodoulides, and Z. Chen, *Self-accelerating Airy Beams: Generation, Control, and Applications*, vol. 170 of *Springer Series in Optical Sciences*, pp. 1–46. Springer, 2012.

[10] N. K. Efremidis and D. N. Christodoulides, "Abruptly autofocusing waves," *Opt. Lett.*, vol. 35, pp. 4045–4047, Dec 2010.

[11] D. G. Papazoglou, N. K. Efremidis, D. N. Christodoulides, and S. Tzortzakis, "Observation of abruptly autofocusing waves," *Opt. Lett.*, vol. 36, pp. 1842–1844, May 2011.

[12] P. Zhang, J. Prakash, Z. Zhang, M. Mills, N. Efremidis, D. Christodoulides, and Z. Chen, "Trapping and guiding microparticles with morphing autofocusing airy beams," *Optics Letters*, vol. 36, no. 15, pp. 2883–2885, 2011. cited By (since 1996) 15.

[13] Y. Kaganovsky and E. Heyman, "Wave analysis of airy beams," *Opt. Express*, vol. 18, pp. 8440–8452, Apr 2010.

[14] R. Gilmore, *Catastrophe Theory for Scientists and Engineers*. Dover books on advanced mathematics, Dover Publications, 1993.

[15] I. Chremmos, N. K. Efremidis, and D. N. Christodoulides, "Pre-engineered abruptly autofocusing beams," *Opt. Lett.*, vol. 36, pp. 1890–1892, May 2011.

[16] E. Greenfield, M. Segev, W. Walasik, and O. Raz, "Accelerating light beams along arbitrary convex trajectories," *Phys. Rev. Lett.*, vol. 106, p. 213902, May 2011.

[17] I. D. Chremmos, Z. Chen, D. N. Christodoulides, and N. K. Efremidis, "Abruptly autofocusing and autodefocusing optical beams with arbitrary caustics," *Phys. Rev. A*, vol. 85, p. 023828, Feb 2012.

[18] H. Hristov, *Fresnel zones in wireless links, zone plate lenses and antennas*. Artech House antennas and propagation library, Artech House, 2000.

[19] H. Trzaska, *Electromagnetic Field Measurements in the Near Field*. Noble Pub., 2001.

[20] V. Coskun, K. Ok, and B. Ozdenizci, *Near Field Communication (NFC): From Theory to Practice*. Wiley, 2012.

[21] J. Goodman, *Introduction To Fourier Optics*. McGraw-Hill physical and quantum electronics series, Roberts & Company, 2005.

[22] L. Felsen and N. Marcuvitz, *Radiation and Scattering of Waves*. IEEE Press Series on Electromagnetic Waves, Wiley, 1994.

[23] M. Abramowitz and I. Stegun, *Handbook of Mathematical Functions: With Formulas, Graphs, and Mathematical Tables*. Applied mathematics series, Dover Publications, 1965.

[24] C. Balanis, *Antenna Theory: Analysis and Design*. Knovel library, John Wiley & Sons, 2005.

[25] L. Froehly, F. Courvoisier, A. Mathis, M. Jacquot, L. Furfaro, R. Giust, P. A. Lacourt, and J. M. Dudley, "Arbitrary accelerating micron-scale caustic beams in two and three dimensions," *Opt. Express*, vol. 19, pp. 16455–16465, Aug 2011.

[26] I. Kaminer, R. Bekenstein, J. Nemirovsky, and M. Segev, "Nondiffracting accelerating wave packets of maxwell's equations," *Phys. Rev. Lett.*, vol. 108, p. 163901, Apr 2012.

[27] P. Zhang, Y. Hu, T. Li, D. Cannan, X. Yin, R. Morandotti, Z. Chen, and X. Zhang, "Nonparaxial mathieu and weber accelerating beams," *Phys. Rev. Lett.*, vol. 109, p. 193901, Nov 2012.

[28] I. D. Chremmos, Z. Chen, D. N. Christodoulides, and N. K. Efremidis, "Bessel-like optical beams with arbitrary trajectories," *Opt. Lett.*, vol. 37, pp. 5003–5005, Dec 2012.

[29] J. Zhao, P. Zhang, D. Deng, J. Liu, Y. Gao, I. D. Chremmos, N. K. Efremidis, D. N. Christodoulides, and Z. Chen, "Observation of self-accelerating bessel-like optical beams along arbitrary trajectories," *Opt. Lett.*, vol. 38, pp. 498–500, Feb 2013.